Simulation of Atmospheric Flow Characteristics and Selection of Models for Artificial Simulated Fog-Haze Environment

HAIMING ZHENG[ID], SHUAI LI[ID], AND JIAWEI YIN[ID]

Department of Mechanical Engineering, North China Electric Power University, Baoding 071003, China

Corresponding author: Haiming Zheng (haimingzheng@163.com)

ABSTRACT The devices for artificial flashover experiment should be constructed and the stability of the airflow field is the key to construct it. This work presents a methodology of constructing three models respectively without blades, with straight blades and with curved blades, coupled for artificial simulated fog-haze environment with computational fluid dynamics (CFD), to predict the impact of the rotating blades on the flow velocities in the enclosed environment by simulation. Atmospheric flow characteristics and variation of flow velocities were analyzed, and the influences of different rotating blades on flow velocities were compared to get the related simulation results in three models. It is showed that the flow velocities increase with the increase of device's Y coordinate. Compared with the variation of flow velocities in the model without blades, it is confirmed that the variation of flow velocities in two models with blades is reduced relatively, in which the variation of flow velocities in the model with straight blades is lower and more stable. Therefore, the designed model with straight blades will be developed for artificial flashover experiment.

INDEX TERMS Simulated fog-haze environment, computational fluid dynamics (CFD), atmospheric flow characteristics, blades.

I. INTRODUCTION

Fog-haze is the combination of sprays and particles, and its essence is the special weather phenomenon of air pollution. Nowadays, the frequent fog-haze weather accelerates contaminant deposition on the transmission equipment's insulator surfaces, which caused the frequent occurrence of flashover. Thus, the significant scientific application value can be achieved by researching the influence laws of fog-haze environment on flashover and finding corresponding solutions [1]. Nevertheless, natural fog-haze environment is a random and unpredictable phenomenon that the parameters of fog-haze are changing all the time and its conditions cannot be controlled by human beings [2]. Accordingly, it is very difficult to further research in natural atmospheric environment and we need to develop an experimental platform that can simulate fog-haze more effectively.

The associate editor coordinating the review of this manuscript and approving it for publication was Xiping Hu[ID].

In several years, a large number of artificial fog-haze experimental platforms were built to research insulator flashover experiment. Guo *et al.* [3] constructed a Plexiglas artificial fog-haze chamber and mixed kieselguhr, calcium sulphate ($CaSO_4$) and ammonium sulphate ($(NH_4)2SO_4$) in different particle sizes with ultrasonic fog to simulate the fog-haze environment. Sungnam and Park [4] adopted natural particles for pollutants disposition and analyzed the effects of dirty dust on insulators in coastal and industrial areas. Ravelomanantsoa *et al.* [5] set up a test platform in the field and analyzed the relationship between the wind speed and the density of the contamination components. Hall *et al.* [6] built a laboratory platform to study the influence of wind, electric field and insulator geometries on the contamination deposition on insulator surfaces. Chisholm *et al.* [7] developed the flashover experimental method for insulators under salt spray, cold fog-haze conditions. Castro *et al.* [8] made artificial rainfall and analyzed the effect of rainfall on insulators' surface contamination.

Therefore, many researchers addressed large number of works on the influence of haze deposition on the external insulation of power transmission and transformation equipment by constructing many kinds of artificial fog-haze experimental platforms. However, there are differences between the simulated and natural fog-haze, which contributed to a large difference in the experimental results, and the main reason is the simulation device designed by predecessors is difficult to ensure a stable haze environment, that is satisfy appropriate temperature and pressure and make air, water vapor and atmospheric aerosol particle coexist to meet the relevant humidity, particle concentration and other haze indicators [9]. If the atmospheric flow characteristics in the artificial fog-haze device can be simulated before designing a fog-haze environment device, data reference could be provided the simulated device's design to ensure that the artificial haze experiments are more consistent with the natural atmospheric environment.

Because of recent developments in computer technology, computational fluid dynamics (CFD) became a powerful tool for studying atmospheric flow characteristics in many cases [10], [11]. Many researchers have digitally analyzed different variation of atmospheric flow by mathematical modeling and numerical simulation. Rodio et al. [12] performed a stochastic analysis of a cavitating flow evolving in a Venturi configuration by using the CFD solver. Dular et al. [13] adopted Fluent 6.1.18 to perform RANS 3D simulation of the cavitation flow in hydraulic machines to describe the generation and evaporation of vapour phase. Tominaga and Stathopoulos [14] designed the simple models for analyzing the influence of turbulence models in the prediction of dispersion around isolated building.

CFD is also widely used in the simulation of insulator flashover in atmospheric environment. Based on the finite element method for predicting both DC and AC critical flashover voltage of polluted porcelain and glass insulators. Jabbari et al. [15] adopted the AR model based on the finite element method to predict both DC and AC critical flashover voltage of polluted porcelain and glass insulators. Ilhan et al. [16] used finite element method for simulating polluted insulators both at power frequency and at lightning impulse voltages. Liu et al. [17] designed the CFD simulation of high-velocity airflow to confirm the leading role of high-velocity airflow and the low pressure airflow. Vasile-Mircea et al. [18] developed 3D electric insulators models that implemented in a drying simulator to describe the heat and mass transfer processing around the electric insulator. However, these simulations mainly concentrated on the influence of particle diameter, haze concentration, etc. on insulator flashover incidents. Few papers simulated the effects of wind speed by computational fluid dynamics, which is not enough to describe the variation of atmospheric flow characteristics only by the wind speed.

Therefore, there is a lack of literature on the numerical simulation of atmospheric flow characteristics around insulators. The present study is aimed at establishing the different haze simulation models with different blades and simulating the characteristics of atmospheric flow and predicting the variation of flow rate in the models by CFD Fluent. The effects of different blades rotation on the atmospheric flow are compared to obtain the related simulation results to provide a reliable theoretical basis for the design of the device for simulated fog-haze environment. This study is based on a set of CFD code, namely Fluent 14.5 and its results are got by designing the relevant code and parameters.

II. NUMERICAL SIMULATION METHOD

A. THE GOVERNING EQUATIONS OF AIRFLOW

Airflow is seen as a continuous phase and the Euler description are used in this paper. The airflow is governed by the laws of conservation of physics. The usual laws of conservation include laws of conservation of mass, laws of conservation of energy and laws of conservation of momentum. These laws of conservation are expressed by continuity equations and Reynolds equations (*N-S* equations) in fluid mechanics. In the experiment, the governing equations describing the airflow characteristics in the device are expressed in Cartesian coordinates, such as (1) and (2).

Continuity equation can be written as:

$$\frac{\partial \rho}{\partial t} + \frac{\partial(\rho u)}{\partial x} + \frac{\partial(\rho v)}{\partial y} + \frac{\partial(\rho w)}{\partial z} = 0 \tag{1}$$

N-S equations for Compressible viscous fluid can be written as:

$$\rho \frac{du}{dt} = \rho f_x - \frac{\partial p}{\partial x} + \frac{\partial}{\partial x}\left\{\mu\left[2\frac{\partial u}{\partial x} - \frac{2}{3}\left(\frac{\partial u}{\partial x} + \frac{\partial v}{\partial y} + \frac{\partial w}{\partial z}\right)\right]\right\}$$
$$+ \frac{\partial}{\partial y}\left[\mu\left(\frac{\partial u}{\partial y} + \frac{\partial v}{\partial x}\right)\right] + \frac{\partial}{\partial z}\left[\mu\left(\frac{\partial w}{\partial x} + \frac{\partial u}{\partial z}\right)\right]$$
$$\rho \frac{dv}{dt} = \rho f_y - \frac{\partial p}{\partial y} + \frac{\partial}{\partial y}\left\{\mu\left[2\frac{\partial v}{\partial y} - \frac{2}{3}\left(\frac{\partial u}{\partial x} + \frac{\partial v}{\partial y} + \frac{\partial w}{\partial z}\right)\right]\right\}$$
$$+ \frac{\partial}{\partial z}\left[\mu\left(\frac{\partial v}{\partial z} + \frac{\partial w}{\partial y}\right)\right] + \frac{\partial}{\partial x}\left[\mu\left(\frac{\partial u}{\partial y} + \frac{\partial v}{\partial x}\right)\right]$$
$$\rho \frac{dw}{dt} = \rho f_z - \frac{\partial p}{\partial z} + \frac{\partial}{\partial z}\left\{\mu\left[2\frac{\partial w}{\partial z} - \frac{2}{3}\left(\frac{\partial u}{\partial x} + \frac{\partial v}{\partial y} + \frac{\partial w}{\partial z}\right)\right]\right\}$$
$$+ \frac{\partial}{\partial x}\left[\mu\left(\frac{\partial w}{\partial x} + \frac{\partial u}{\partial z}\right)\right] + \frac{\partial}{\partial y}\left[\mu\left(\frac{\partial v}{\partial z} + \frac{\partial w}{\partial y}\right)\right] \tag{2}$$

where ρ represents density (kg/m^3), x, y and z represents position coordinates, u, v, w represents the three speed components along x, y and z axis, μ represents dynamic laminar viscosity, and p represents pressure of fluid.

The fluid is rotated in a device with a cylindrical structure, it is more appropriate to make use of the cylindrical coordinate system to describe fluid motion. The steady motion of a fluid in an incompressible system is considered, and its continuous equation in a cylindrical coordinate system can be written as (3):

$$\frac{1}{r}\frac{\partial u_\theta}{\partial \theta} + \frac{\partial u_\theta}{\partial r} + \frac{\partial u_\theta}{\partial z} + \frac{u_r}{r} = 0 \tag{3}$$

B. SELECTION OF TURBULENCE MODEL

It is now known that many factors, such as turbulence models, can influence the accuracy and reliability of a CFD simulation, and many research have assessed the effect of different such factors on numerical solutions [19], [20].

In FLUENT, there are three main k-ε turbulence models: the standard (STD) k-ε turbulence model [21], the RNG k-ε turbulence model [22] and the Realizable k-ε model [23]. In practical operation, the STD k-ε model is remaining the most widely used approaches to modeling wind engineering and atmospheric dispersion problems [24]. In this paper, the STD k-ε model is chosen as the applied turbulence model. By applying the STD k-ε model and assuming constant pressure and shear stress and zero vertical velocities, the turbulent kinetic energy equation of standard k-ε model can be written as (4):

$$\frac{\partial(\rho k)}{\partial t} + \frac{\partial(\rho k u_i)}{\partial x_i} = \frac{\partial}{\partial x_j}\left[\left(\mu + \frac{\mu_t}{\sigma_\varepsilon}\right)\frac{\partial \varepsilon}{\partial x_j}\right]$$
$$+ C_{1\varepsilon}\frac{\varepsilon}{k}P_k + C_{2\varepsilon}\rho\frac{\varepsilon^2}{k} \quad (4)$$

The turbulent kinetic energy dissipation equation of standard k-ε model can be written as (5):

$$\frac{\partial(\rho k)}{\partial t} + \frac{\partial(\rho k u_i)}{\partial x_i} = \frac{\partial}{\partial x_j}\left[\left(\mu + \frac{\mu_i}{\sigma_k}\right)\frac{\partial k}{\partial x_j}\right] + P_k - \rho\varepsilon \quad (5)$$

where k is turbulent kinetic energy, which indicates that the variation of velocities fluctuation, unit is m^2/s^2, ε is turbulent kinetic energy dissipation, indicating the rate of dissipation of velocities fluctuation in flow, and unit is m^2/s^3.

With the STD k-ε model the eddy viscosity is related to the turbulence kinetic energy (k) and its rate of dissipation (ε) [25] defined as (6):

$$\mu_t = C_\mu \rho \frac{k^2}{\varepsilon} \quad (6)$$

where P_k represents turbulent outcome of viscous force and buoyancy, σ_k and σ_ε represents turbulent diffusion terms the model has five constants, i.e., σ_k, σ_ε, $C_{1\varepsilon}$, $C_{2\varepsilon}$, C_μ, their standard values given by Pope [26] are $\sigma_k = 1.0$, $\sigma_\varepsilon = 1.3$, $C_{1\varepsilon} = 1.44$, $C_{2\varepsilon} = 1.92$, $C_\mu = 0.09$.

III. CHARACTERISTIC OF PARTICLE MOTION

The gravity of particle can be calculated as (7):

$$F_1 = m_p g = \frac{\pi}{6}\rho d_p^3 g \quad (7)$$

When particles are suspended in the atmosphere, buoyancy equals weight of air in the same volume, so buoyancy can be calculated as (8):

$$F_2 = mg = \frac{\pi}{6}\rho d_p^3 g \quad (8)$$

The resistance of particles in air is related to the relative velocities of particles and air flow, the size of particle projection cross section and the coefficient of resistance can be calculated as (9):

$$F3 = \psi\frac{\pi}{4}d_p^2\frac{v^2}{2}\rho = \psi\frac{\pi d_p^2 \rho v^2}{8} \quad (9)$$

where ψ is the coefficient of drag force, v is the relative velocities of particles ($|u\text{-}u_p|$), the rest of the parameters are same as above.

When the particles are in the interaction of three acting forces, they settled and the velocities of particles increase. When the resistance, buoyancy, gravity are in balance, i.e. $F_1 - F_2 - F_3 = 0$, the particles would settle in constant speed and the velocities at this point can be defined as particle gravity settling velocities or Stokes velocities v_s, can be calculated as (10):

$$vs = \sqrt{\frac{4dp(\rho p - \rho)g}{3\psi\rho}} \quad (10)$$

The flow resistance coefficient ψ is relevant to the flowage of particles in the air flow, i.e. laminar or turbulent. The shape of the particles may also affect the flow resistance coefficient.

The flow state of particles is determined by the relative Reynolds number (R_{ep}) of particles. Furthermore, for particles motion, generally R_{ep} is less than 1, and when R_{ep} is less than 0.5, the resistance of spherical particles can be calculated as (11):

$$F3 = 3\pi\mu d_p v \quad (11)$$

Equation (11) can also be called as Stokes formula. When R_{ep} is less than 0.5, the particles deformed by the viscous resistance opposite to the gravity. The 1/3 of resistance F_3 is created by particle deformation; rest of it is friction resistance. Therefore, the resistance coefficient can be derived in 12, the derived equation can be written as (12):

$$\psi = \frac{24\mu}{d_p v} = \frac{24}{R_{ep}} \quad (12)$$

In (12), resistance is closely related to the velocities of particle. Nevertheless, when the Reynolds number is large, the effect of inertia force must be considered, and the resistance and speed are not linear.

If the Reynolds number is large, the flow is no longer laminar as the particles tend to move in a random manner. In conclusion, for large particles, particle sedimentation accelerated by gravity is particularly obvious and the effect of gravity on the particle size increasing in general.

IV. MODELING AND BOUNDARY CONDITIONS
A. MODELING DESCRIPTION AND MESHING GENERATION

In this paper, we prepared three small cylindrical testing devices. In Fig.1, it can be seen that three-dimensional models of three devices were constructed and there are four airway tubes, four supporting frames, an outlet and three entrances of probe in the model. The device is 1.8m high and has a
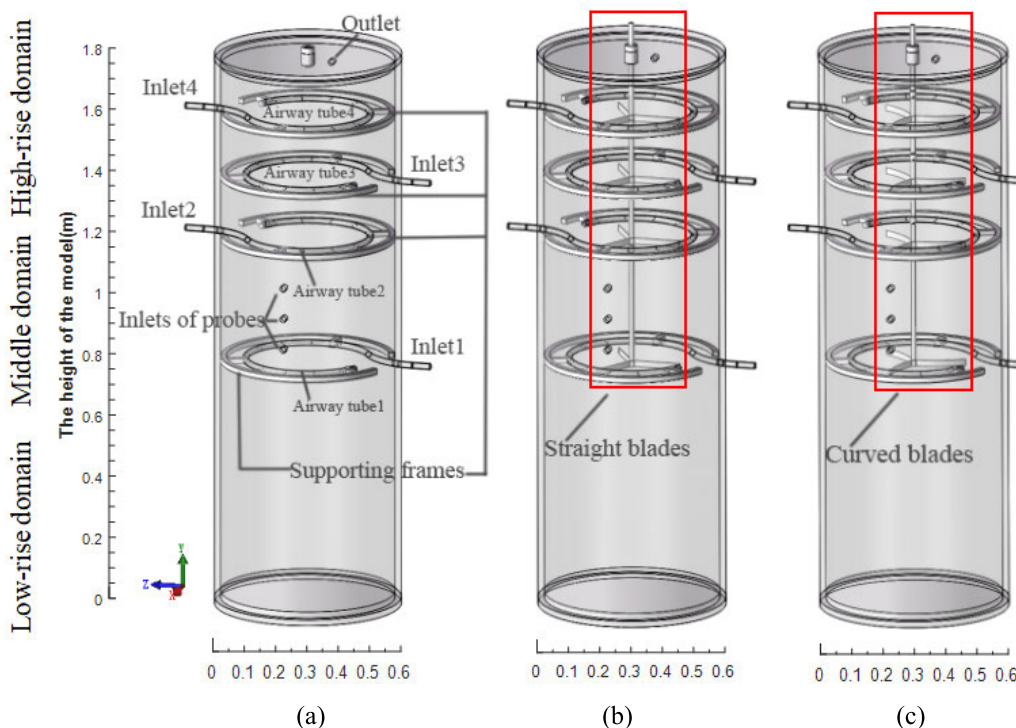
FIGURE 1. The structure of simulated fog-haze device that without blades (a), with straight blades (b) and with curved blades (c).

diameter of 0.6m. The four air ducts are placed at the height of 0.8m, 1.2m, 1.4m and 1.6m of the device.

The airway is a circular cavity with a diameter of 0.4m. The thickness of inner cavity is 1mm. Its ring-shaped feature can prevent the particles from flowing back. Airway tube is used for introducing fog-haze gas, supporting frame is used for supporting airway tube, the outlet is used to remove waste gas and the entrance of probe is used to put the device that detecting the property of gas. It is obviously that the only difference is the rotating blades that adjusting the airflow of device. The rotating blades are placed at the same height as each vent pipe. It is shown that the model in Fig.1 (a) is without blades, the model in Fig.1 (b) is with straight blades and the model in Fig.1(c) is with curved blades. Based on the difference of blades, the simulation models in Fig.1 (a), Fig.1(b) and Fig.1(c) are simply called as without blades, With straight blades and ' With Curved Blades' respectively.

Exploring the role of the shape of the haze device and the profile of the blade in the simulation process, that is also the main purpose of our simulation. To simulate the characteristics of these atmospheric flows and the varia- tion of the flow velocities, the fluid domains of relevant models are constructed in this paper, and these models are imported into the ICEM for meshing. A systematical sensi- tivity test for the mesh number was conducted by examining the dependence of numerical solutions on mesh number. As a compromise between numerical accuracy and model structures, structured tetrahedra cells are used to build fluid domains. Table 1 presents the domain extent of three models

TABLE 1. The domain extent of three devices in 3D coordinates.

Xmin (m)	-0.356	Xmax (m)	0.356
Ymin (m)	0	Ymax (m)	1.76
Zmin (m)	-0.28	Zmax (m)	0.28

TABLE 2. Mesh information of computational domains.

	Devices		
	Without blades	with straight blades	with curved blades
Number of nodes	785975	964348	972747
Number of elements	4121787	4460719	4472106
Tetrahedra	4121787	4375222	4382037
Wedges	0	456	336
Hexahedra	0	85041	89733

in three-dimensional coordinates. Table 2 illustrates the mesh information of computational domain in these devices.

B. BOUNDARY CONDITION SETTINGS

Table 3 indicates the setting of boundary conditions in fluid domains. The parameter settings of boundary condition are shown in Table 3. It can be seen that the inlet flow velocity in numerical simulation can be set as 1m/s and the flow direction is perpendicular to the entrance of the device. The outlet pres- sure can be set as 0.996kpa and the distribution of it can be considered as uniform. In the experiment, temperature of air
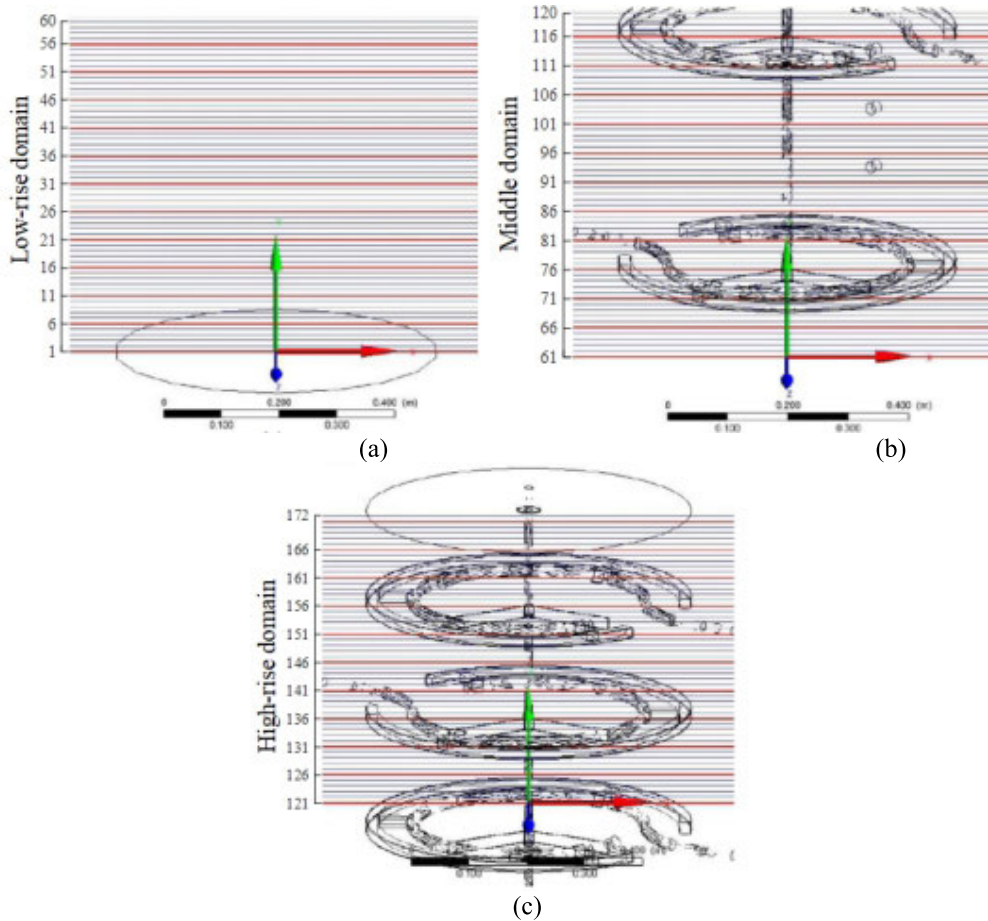
FIGURE 2. Sampling lines at X-direction in low-rise domain (a), middle domain (b) and high-rise domain (c).

can be set 298K (room temperature), which take account the k-ω function based on the automatic wall treatment model.

For all simulations conducted in this study, the pressure velocities coupling was held by the SIMPLE algorithm, the pressure interpolation was second order, and both the convention and diffusion terms were treated by second-order accuracy discretization schemes. Convergence was assumed to be achieved when all the scalar residuals reached 10^{-5} and the solutions of the calculation were stable over dozens of iterations.

V. RESULTS AND DISCUSSION

A. SELECTION OF SAMPLING AREAS

Given that three models have the same appearance structures except for blades, the paper presents the schematic views of sampling domains in the model with straight blades, the same sampling domains of the models without blades and with straight blades are no longer listed. It can be seen from Fig.1 that based on the difference of Y coordinate, the 3D fluid domain can be divided into three parts. The domain from the Y coordinate of 0-0.6m, 0.6-1.2m and 1.2-1.72m can be named as 'Low-rise domain', 'Middle domain', and 'High-rise domain' respectively.

TABLE 3. The parameter settings of boundary condition.

Main parameters	Setting values
Inlet boundary condition	Velocities-inlet
Inlet velocities (m/s)	1
turbulence intensity	5%
turbulence viscosity Ratio	10
Average particle size (m)	2×10^{-6}
Temperature (K)	298
Outlet boundary condition	Pressure-outlet
turbulence model	Standard
Turbulent kinetic energy (m^2/s^2)	3.75×10^{-3}
Turbulent dissipation Rate (m^2/s^3)	8.66×10^{-3}
Initial velocities (m/s)	0
Rotational velocities/(rpm)	100

On the direction of the coordinate and perpendicularing to the bottom of model, 'XY Plane' and 'YZ Plane' are constructed separately, which are adopted to calculate the characteristics of three models.

Compare the difference of from these contours. To simulate the variation of the velocity streamlines' direction, 50 green sampling points are selected evenly on 'XY Plane' and 'YZ Plane'.
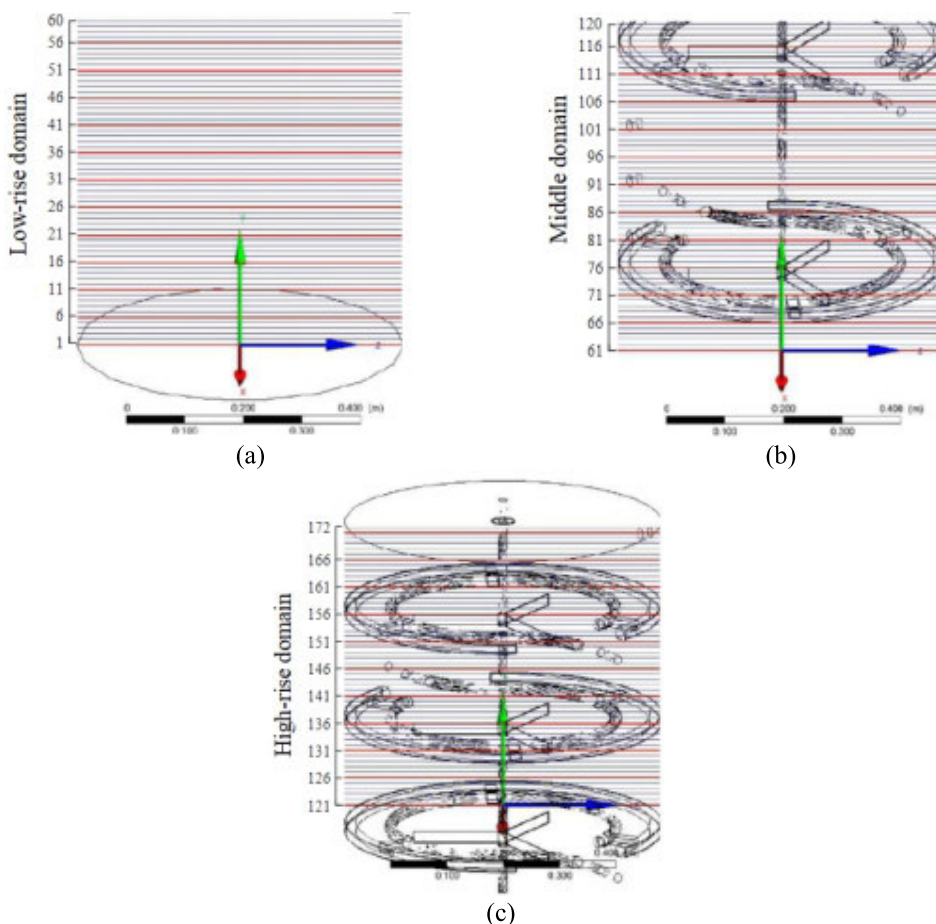
FIGURE 3. Sampling lines at Z-direction in low-rise domain (a), middle domain (b) and high-rise domain (c).

TABLE 4. The setting of solution methods.

Pressure-velocities Coupling	
Scheme	SIMPLE algorithm
Spatial Discretization	
Gradient	Least Squares Cell Based
Pressure	Standard
Momentum	Second order wind
Turbulent kinetic energy	First order wind
Turbulent dissipation Rate	First order wind

TABLE 5. The setting of line1, line2 and line3.

	Start-point coordinates			End-point coordinates		
	x(m)	y(m)	z(m)	x(m)	y(m)	z(m)
Line1	-0.2	0	0	-0.2	1.7	0
Line2	0.1	0	0.1	0.1	1.7	0.1
Line3	0.19	0	-0.18	0.19	1.7	-0.18

The schematic views of four sampling planes as parallel-ing to the bottom, which are separately at the Y coordinate of 0.4m (a), 1m (b), 1.5m (c) and 1.6m (d). The plane (a) and (b) represent as 'Low-rise domain' and 'Middle domain'. The plane (c) and (d) represent as 'High-rise domain'. These sampling planes can be used to collect the corresponding contour maps and compare the lateral flow velocities distribution of three devices in different domains.

Table 5 shows the starting and ending coordinates of line1, line2 and line3 and 1000 points are selected on three lines as sampling points respectively. To analyze the vertical flow

velocity changes at different domains, these three longitudinal sampling lines are adopted.

From Fig.2 and Fig.3, it can be seen that 172 sampling lines at the X axis and Z axis respectively are chosen along the Y coordinate from 0m to 1.71m in 3D coordinates evenly and 1000 points are evenly sampled at 1000 points on each sampling line. In Table 6, it can be indicated that these sampling lines are classified in 'Low-rise domain', 'Middle domain' and 'High-rise domain' for the variation of Y coordinate respectively. By collecting these data on sampling lines, maximum velocities and average velocities can be obtained to make the comparison of the vertical velocity variation of three models.

B. THE CHARACTERISTICS OF STREAMLINES
By simulating the selected sampling points on 'XZ plane' and 'YZ Plane', the distribution of streamlines are presented
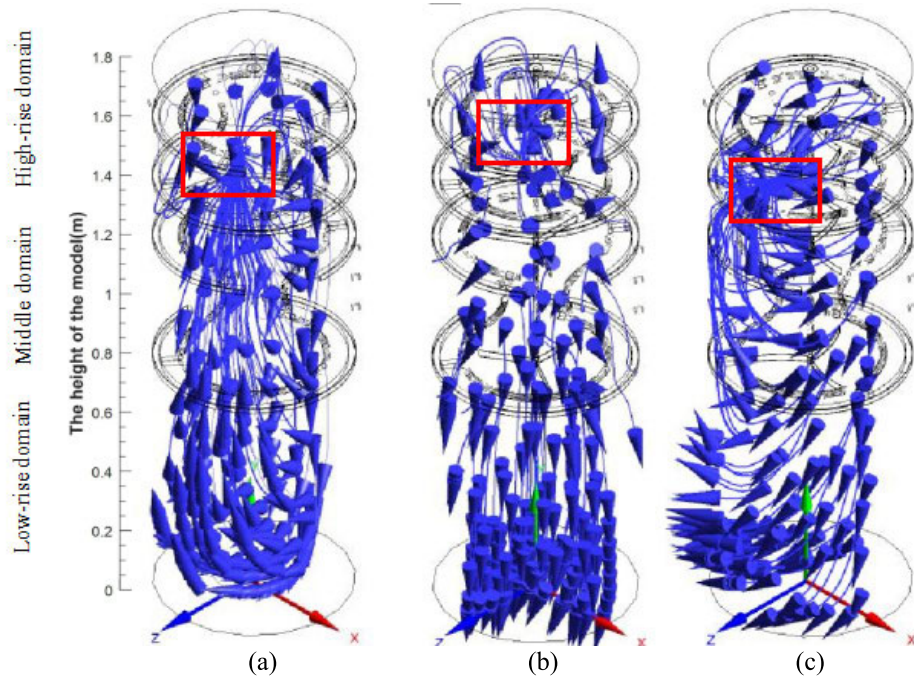
FIGURE 4. The distribution of streamlines in three models: (a) without blades; (b) With straight blades; (c) With curved blades.
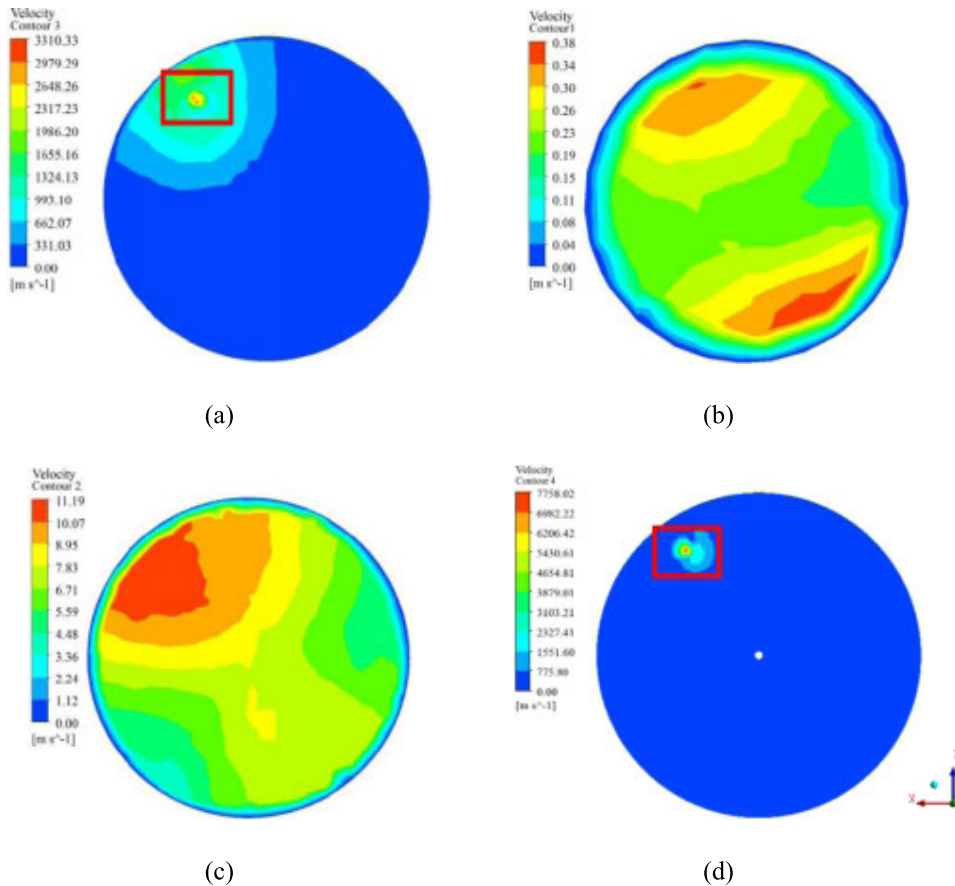
FIGURE 5. The velocity distribution in without blades at the Y coordinate of 0.4m (a), 1m (b), 1.5m(c) and 1.6m (d).

in Fig.4. From the red frames in Fig.4, it can be seen that there is similarities in three models, which is with a concentrated rotating eddy in high-rise domain separately. The eddy current's center points are respectively at the Y coordinate of 1.35m, 1.5m and 1.3m in three models. Nevertheless, in the direction of the streamlines, there is a big
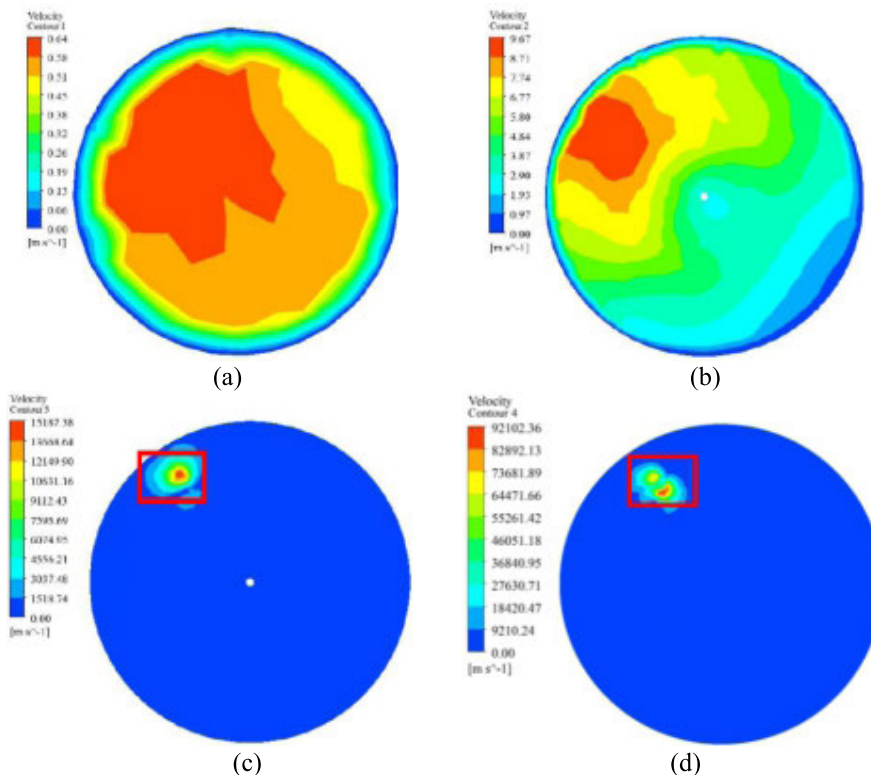
FIGURE 6. The velocity distribution in with straight blades at the Y coordinate of 0.4m (a), 1m (b), 1.5m(c) and 1.6m (d).
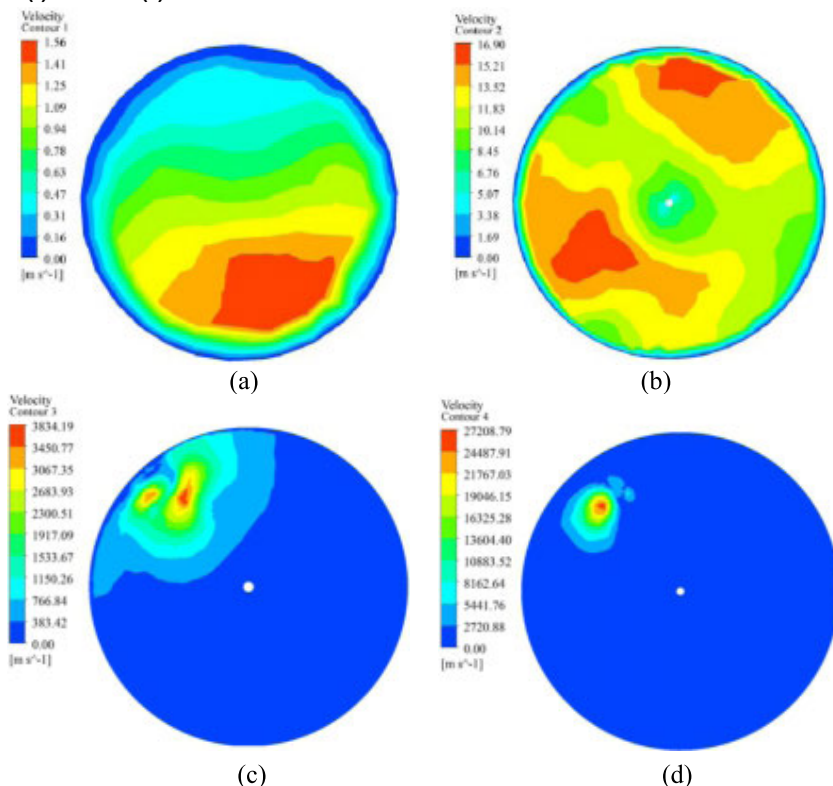

FIGURE 7. The velocity distribution in With curved blades at the Y coordinate of 0.4m (a), 1m (b), 1.5m(c) and 1.6m(d).

difference between the three models. In without blades, the streamlines diverge from the eddy current's center at high-rise domain, the streamlines are basically moving downward at the Middle domain and up flow back in low-rise domain. In with straight blades, and the streamlines diverged around at high-rise domain and Middle domain, and move downward

TABLE 6. The setting of X-direction sampling lines and Z-direction sampling lines.

		Start-point coordinates			End-point coordinates		
		x(m)	y(m)	z(m)	x(m)	y(m)	z(m)
X-direction Sampling Lines	Low-rise Domain		0-0.6			0-0.6	
	Middle Domain	-0.356	0.6-1.2	0	0.356	0.6-1.2	0
	High-rise Domain		1.2-1.71			1.2-1.71	
Z-direction Sampling Lines	Low-rise domain		0-0.6			0-0.6	
	Middle domain	0	0.6-1.2	0.28	0	0.6-1.2	0.28
	high-rise domain		1.2-1.71			1.2-1.71	

TABLE 7. The range of flow velocities in the fluid domains.

Simulated fog-haze devices	Minimum velocity	Maximum velocities
without blades		4.98×10^7 m/s
With straight blades	0m/s	7.952×10^6 m/s
With curved blades		1.445×10^7 m/s

in low-rise domain. In With curved blades, the streamlines gather to the eddy current's center at High-rise domain, are basically upwardly back to the eddy current's center at Middle domain and move horizontally in low-rise domain.

C. THE CHARACTERISTICS OF FLOW VELOCITIES

1) THE RANGE OF FLOW VELOCITIES IN THE FLUID DOMAINS

Table 7 illustrates the ranges of non-dimensional instantaneous flow velocities in the fluid domains of three models. It can be seen that compared with the maximum velocities in without blades, the maximum velocities in the devices with straight blades and with curved blades decreased by 84.03% and 70.98% separately.

D. THE CHARACTERISTICS OF TRANSVERSE VELOCITIES

The transverse velocities distribution predicted by the model at different Y coordinates including Y=0.4m, 1m, 1.5m and 1.6m are illustrated in Fig.5, Fig.6 and Fig.7. At a Y coordinate of 0.4m and 1m, the range of flow velocities is low and the distribution of flow velocities is more uniform. At a Y coordinate of 1.5m and 1.6m, the range of flow velocities is very high, the distribution of flow velocities are very nonuniform and the maximum velocities are respectively near (0.1,1.5,0.15) and (0.1,1.6,0.15) in three-dimensional coordinate. The maximum velocities of each contour are summarized in Table 7. At a Y coordinate of 0.4m and 1m, the maximum velocities are low and close to each other in three models. At the Y coordinate of 1.5m, the maximum velocity in with straight blades is much larger than that in without blades and with curved blades. At the Y coordinate of 1.6m, the maximum velocities in with curved blades are
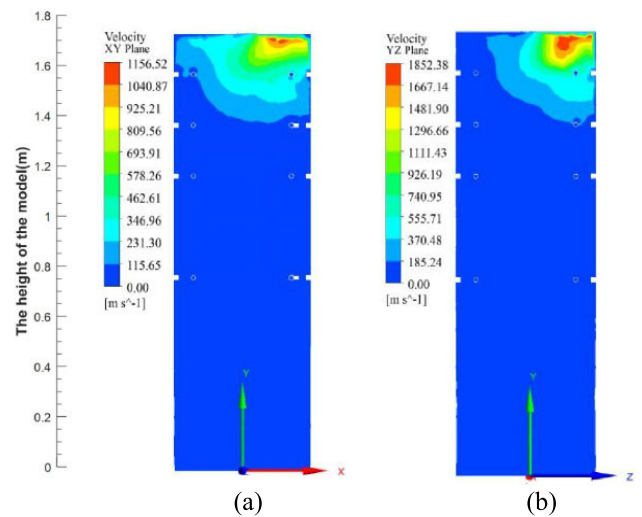

(a)   (b)

FIGURE 8. Longitudinal flow velocity distribution in without blades.

much larger than without blades and with straight blades. The maximum velocities increase as Y coordinate increase in without blades and With curved blades and is closed at Y coordinates of 0.4m, 1m and 1.5m except that at the Y coordinate of 1.6m, the maximum velocities in With curved blades is lower than that in without blades. In With straight blades, the maximum velocity at the Y coordinate of 1.5m is higher than that at the Y coordinate of 1.6m.

1) THE CHARACTERISTICS OF LONGITUDINAL VELOCITIES DISTRIBUTION

By simulating the selected sampling planes as 'XY Plane' and 'YZ Plane' in Fig.5, the characteristics of longitudinal velocities distribution in without blades, with straight blades and with curved blades are presented in Fig.8, Fig.9 and Fig.10. From these figures, it can be concluded that comparing to the range of flow velocities at high-rise domain, the range of flow velocities is lower at low-rise domain and middle domain. The distribution of flow velocities at high-rise domain is nonuniform. In without blades, the domain of maximum velocities on XY Plane and YZ Plane are probably
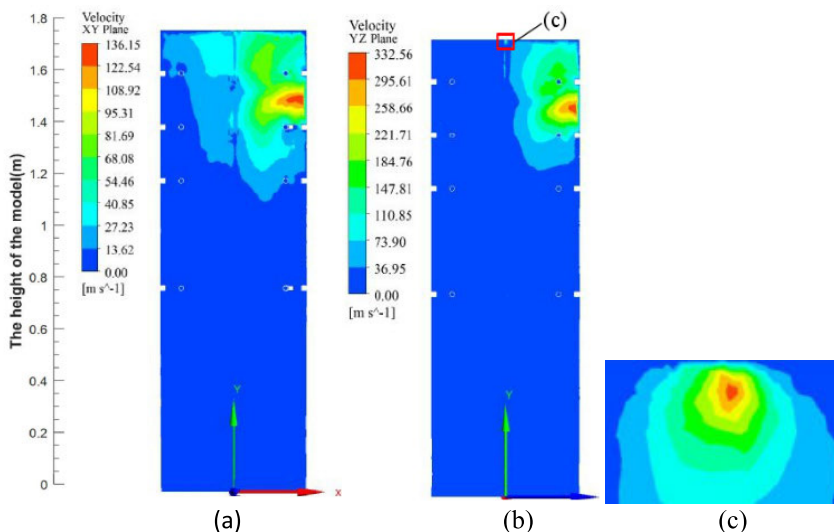
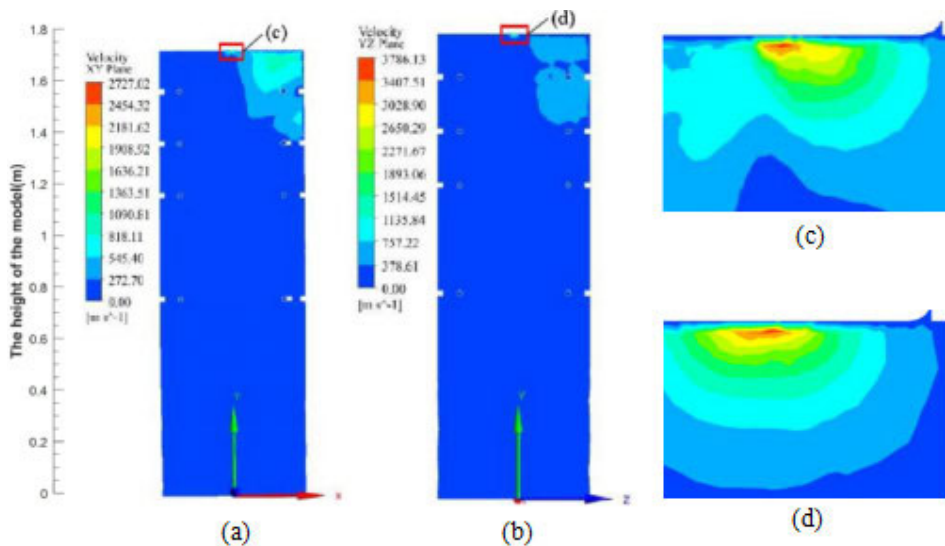**FIGURE 9.** Longitudinal flow velocity distribution in with straight blades.

**FIGURE 10.** Longitudinal flow velocity distribution in with curved blades.

TABLE 8. The maximum velocities of contours.

	0.4m	1m	1.5m	1.6m
Simulated fog-haze models	Maximum velocities(m/s)			
without blades	0.38	11.19	3310.33	92102.36
With straight blades	0.64	9.67	15187.38	7758.02
With curved blades	1.56	16.90	3834.19	27208.79

near (0.11, 1.65, 0) and (0, 1.65, 0.11) respectively. In With straight blades, the domain of maximum velocities on XY.

Plane is probably near (0.11, 1.65, 0), and the domain of maximum velocities on XY Plane is probably near (0, 1.65, 0.11) and (0, 1.7, 0). In With curved blades, the domain of maximum velocities on XY Plane and YZ Plane are

probably near in without blades, the domain of maximum velocities on XY Plane and YZ Plane are all near (0, 1.7, 0) respectively. Table 8 presents the maximum flow velocities of these contours. It can be seen that comparing with the maximum flow velocities in without blades that in With straight blades decreased by 88.23% and that in With curved blades
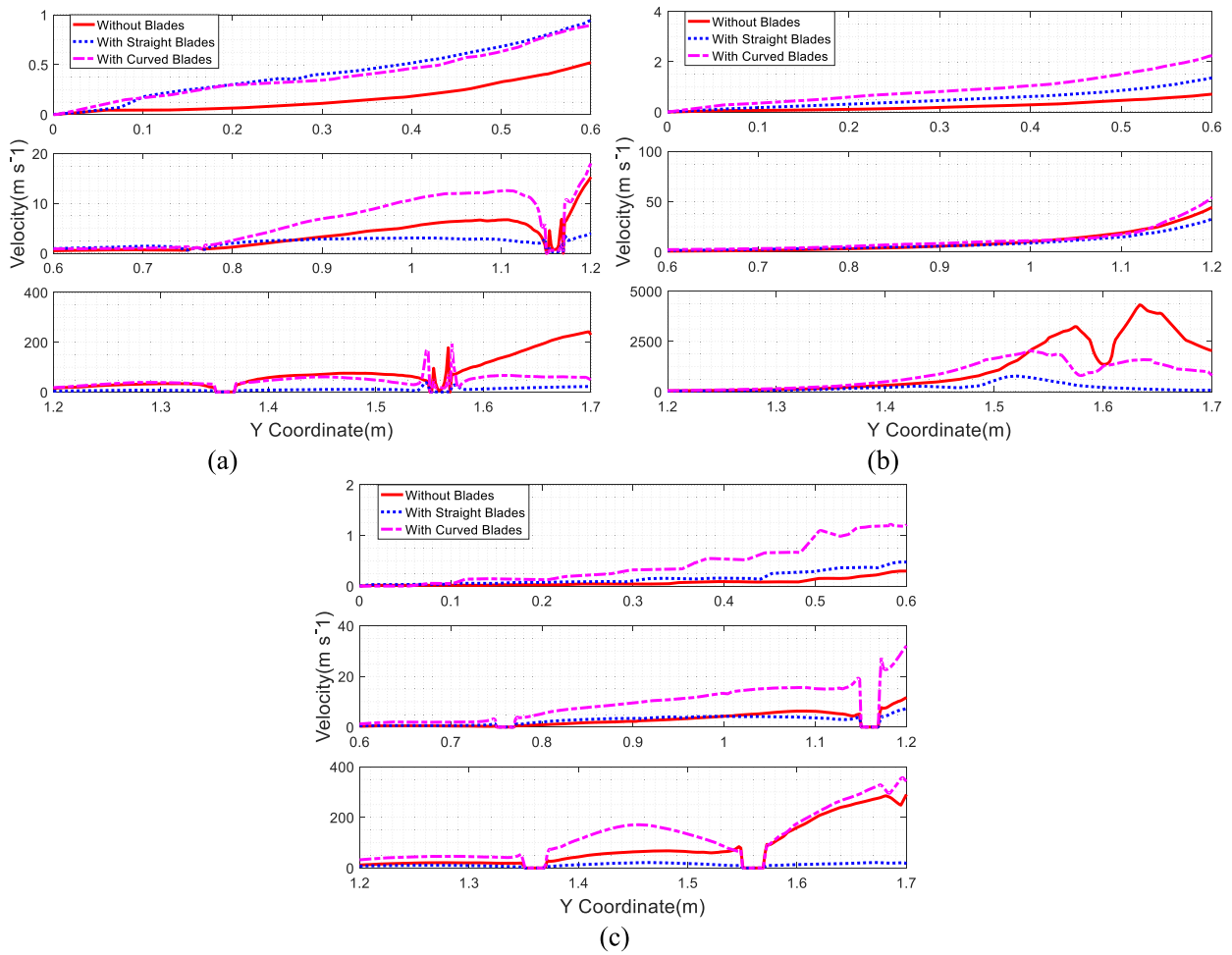
FIGURE 11. The variation of flow velocities on three vertical sampling lines: (a) sampling line 1; (b) sampling line 2; (c) sampling line 3.

increased by 135.80% on XY plane. On the YZ plane, compared with the maximum flow velocities in without blades, the maximum flow velocities in with straight blades and with curved blades decrease by 82.05% and increased by 104.39% respectively.

Fig.11 points out the comparison of non-dimensional velocities on the vertical center plane of the computational domain in three models. Based on the difference of Y coordinates, the characteristics of velocity changes are divided into 'low-rise domain', 'middle domain' and 'high-rise domain'. In low-rise domain, the velocities of three models slowly increased with ascending of the Y coordinate. The velocities are very low and close to each other. Compared with the velocity changes of three sampling lines in without blades and with curved blades, the velocity changes in the device with straight blades are more stable. On the sampling line 1, the velocities near a Y coordinate of 0.76m (airway tube1) and 1.36m (airway tube3) dropped suddenly, which indicated that velocities are low in the airway tubes under the steady conditions. The velocities near a Y coordinate of 1.16m (airway tube2) and 1.56m (airway tube4) are ups and downs,

which indicated that there are unstable turbulence velocities around 1.16m and 1.56m. On the sampling line 2, the velocity changes are stable, which increased with ascending of the Y coordinate from 0m to 1.5m. The velocity changes of without blades and with curved blades fluctuate slightly but the velocity changes of with straight blades. On the sampling line 3, the velocities near a Y coordinate of 0.76m (airway tube1), 1.16m (airway tube2), 1.36m (airway tube3) and 1.56m (airway tube4) dropped to zero suddenly, the reason of which is mainly that the sampling line 3 are very close to the boundary of the fluid domain.

By simulating the selected 172 sampling lines separately, the variation of maximum velocities, average velocities on these sampling lines at X and Z radial line along the Y coordinate are presented in Fig.12 and Fig.13 separately. Whether the sampling lines are at the X direction and Z direction in different models, in the low-rise domain, the velocities variation in with curved blades is the highest, the velocities variation in without blades is the lowest. In the middle domain, the velocities variation in With curved blades is still the highest, the velocities variation of without blades increase more
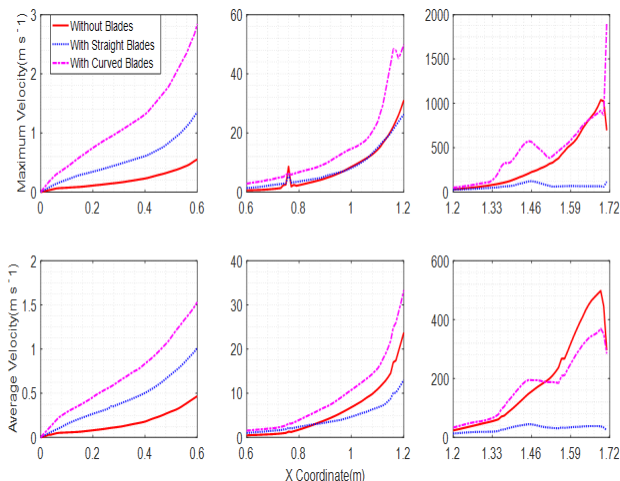
FIGURE 12. Variation of maximum velocities and average velocities in X radial line along the Y coordinate.
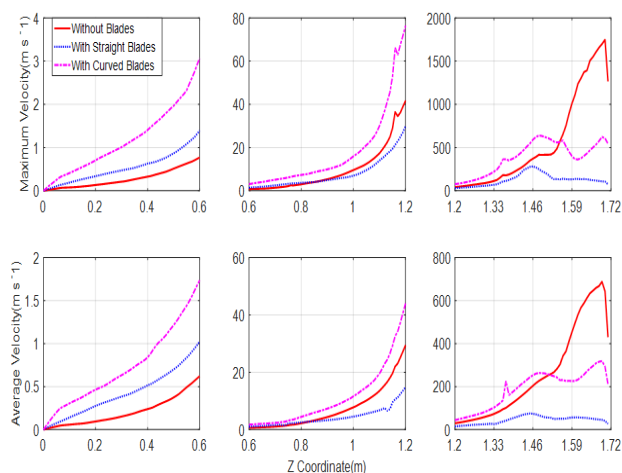
FIGURE 13. Variation of maximum velocities and average velocities in X radial line along the Y coordinate.

quickly and the velocities variation in with straight blades increased slowly. In the high-rise domain, the velocities in with straight blades is very stable and remain approximately constant, the velocities in without blades increase until a Y coordinate of 1.69 m and the velocities in With curved blades are ups and downs.

E. DISCUSSION OF ATMOSPHERIC FLOW CHARACTERISTICS

In this section, based on the standard (STD) k-ε turbulence models designed by Richards and Hoxey [25], we set the boundary conditions to predict the atmospheric flow characteristics and the variation of flow velocities and compare the effect of different blades on the variation of flow velocities in three devices to simulate haze, which are without blades, with straight blades and with curved blades respectively. The results of simulated analysis are proposed below.

Generally, the atmospheric flow characteristics and flow velocities in different fluid domains is different. In the low-rise and middle domains, the velocities in three models are all

low and rise steadily. In the high-rise domains, the velocities are very high and inhomogeneous and there are high-speed vortexes. The boundary conditions, grid meshing and structure of the models are the main reasons for these conditions. It is worth noting that the effects of rotating blades on the flow velocities are obvious. Compared with the flow velocities in without blades and With curved blades, that in With straight blades are more stable in high-rise domain, which indicate that the designed rotating straight blades could stable the flow velocities and reduce the dispersion of particles at some extents. It should also be noted however that the prediction of airflow characteristics.

VI. CONCLUSION

The study presented aimed at proposing a computational method of atmospheric boundary layer turbulence model to simulate the atmospheric flow characteristics and flow velocities, and compare the effect of different blades on variation of flow velocities in three devices without blades, with straight blades and with curved blades. The proposed method is based on the boundary conditions that were defined by Richards and Hoxey [25]. The device with straight blades differs from the other two devices on several points that can be summarized as follows.

1) Generally, the atmospheric flow characteristics and flow velocities in different fluid domains is different. In the low-rise and middle domains, the velocities in three models are all low and rise steadily.
2) In the high-rise domains, velocities are very high and nonuniform and there are high-speed vortexes. For the lateral velocities profile, at the low-rise and middle main, the air velocities is low and close to each other, and at the high-rise domain, the range of flow velocities is very high and the distribution of flow velocities is very nonuniform.
3) Attention should also be given that the effect of the rotating blades at 100 rpm on the flow velocities is significant. The use of the rotating straight blades to solve the unstable flow velocities in the device Without Blades clearly reduces the velocities of both flow and vortex.
4) It is shown that the designed straight blades greatly stabilize the flow velocities in the simulated fog-haze model, especially at high-rise domain, and reduced the settlement of particles to a certain extent. As a result, the designed straight blades is the most suitable for stabilizing the flow velocities in the designed model should be selected to artificial flashover experiment.

However, it also should be considered that for lack of the comparison with corresponding experimental data under same boundary conditions, the reasons for the atmospheric flow characteristics and flow velocities in these models are still unknown, and should be developed in forthcoming studies.

REFERENCES

[1] Y. Sun, Y. Tu, C. Wang, S. Wang, Y. Cheng, Q. Peng, and X. Chen, "Contamination and AC pollution flashover characteristics of insulators under fog-haze environment," in *Proc. IEEE 11th Int. Conf. Properties Appl. Dielectric Mater. (ICPADM)*, Sydney, NSW, Australia, Jul. 2015, pp. 596–599.

[2] A. Calvo, C. Alves, A. Castro, V. Pont, A. Vicente, and R. Fraile, "Research on aerosol sources and chemical composition: Past, current and emerging issues," *Atmos. Res.*, vols. 120–121, pp. 1–28, Feb. 2013.

[3] Y. Guo, X. Jiang, Y. Liu, Z. Meng, and Z. Li, "AC flashover characteristics of insulators under haze–fog environment," *IET Gener., Transmiss. Distrib.*, vol. 10, no. 14, pp. 3563–3569, Nov. 2016.

[4] S. Chun and C. Park, "Analysis of contaminants adhered on polymeric insulator used in coastal and industrial areas," in *Proc. Annu. Rep.-Conf. Electr. Insul. Dielectr. Phenomena (CEIDP)*, Nov. 2008, p. 3, doi: 10.1109/CEIDP.2008.4772915.

[5] N. Ravelomanantsoa, M. Farzaneh, and W. A. Chisholm, "Laboratory investigation of the HV insulator contamination process under winter conditions," in *Proc. Int. Conf. High Voltage Eng. Appl. (ICHVE)*, Nov. 2008, pp. 240–244.

[6] J. Hall and T. Paul, "Wind tunnel studies of the insulator contamination process," *IEEE Trans. Elect. Insul.*, vols. EI-16, no. 3, pp. 180–188, Jun. 1981.

[7] W. Chisholm, K. Ringler, C. Erven, M. Green, O. Melo, Y. Tam, O. Nigol, J. Kuffel, A. Boyer, I. Pavasars, F. Macedo, J. Sabiston, and R. Caputo, "The cold-fog test [for outdoor insulators]," *IEEE Trans. Power Del.*, vol. 11, no. 4, pp. 1874–1880, Oct. 1996.

[8] J. Castro, G. Aponte, V. Sanchez, M. Castro, A. Espinosa, and N. Rosales, "Colombian experience on insulation pollution level measurement applying the ESDD methodology," in *Proc. IEEE/PES Transmiss. Distrib. Conf. Expo., Latin Amer.*, Aug. 2006, pp. 15–18.

[9] Y.-P. Wu, C.-Y. Zhu, G.-L. Feng, and B. L. Li, "Mathematical modeling of Fog-Haze evolution," *Chaos, Solitons Fractals*, vol. 107, pp. 1–4, Feb. 2018.

[10] P. V. Nielsen, "Fifty years of CFD for room air distribution," *Building Environ.*, vol. 91, pp. 78–90, Sep. 2015.

[11] P. Mocho, V. Desauziers, H. Plaisance, and N. Sauvat, "Improvement of the performance of a simple box model using CFD modeling to predict indoor air formaldehyde concentration," *Building Environ.*, vol. 124, pp. 450–459 Nov. 2017.

[12] M. Rodio and P. Congedo, "Robust analysis of cavitating flows in the Venturi tube," *Eur. J. Mech.-B/Fluids*, vol. 44, pp. 88–99, Mar. 2014, doi: 10.1016/j.euromechflu.2013.11.002.

[13] M. Dular, R. Bachert, B. Stoffel, and B. Širok, "Experimental evaluation of numerical simulation of cavitating flow around hydrofoil," *Eur. J. Mech.-B/Fluids*, vol. 24, no. 4, pp. 522–538, Jul. 2005.

[14] Y. Tominaga and T. Stathopoulos, "Numerical simulation of dispersion around an isolated cubic building: Comparison of various types of k–ϵ models," *Atmos. Environ.*, vol. 43, no. 20, pp. 3200–3210, Jun. 2009.

[15] M. Jabbari, C. Volat, and I. Fofana, "Application of a new dynamic numerical model to predict polluted insulator flashover voltage," in *Proc. IEEE Electr. Insul. Conf. (EIC)*, Jun. 2014, pp. 102–106.

[16] S. Ilhan, A. Ozdemir, S. H. Jayaram, and E. A. Cherney, "Numerical and experimental investigation of the effects of pollution on glass suspension-type insulators," *IEEE Trans. Dielectr. Electr. Insul.*, vol. 22, no. 5, pp. 2987–2994, Oct. 2015.

[17] X. Liu, C. Gao, X. Deng, L. Cao, and X. Chen, "The influence of high-velocity airflow on discharge characteristics of electric locomotive roof insulator," in *Proc. IEEE 9th Int. Conf. Properties Appl. Dielectric Mater.*, vols. 1–3, Jul. 2009, pp. 453–456. [Online]. Available: http://ieeexplore.ieee.org/document/5252393/

[18] C. Vasile-Mircea, G. Firuta, and M. L. Mihai, "Modelling and simulation of forced convection drying of electric insulators," *Comput. Aided Chem. Eng.*, vol. 29, pp. 46–50, 2011.

[19] R. Löhner, J. R. Cebral, F. E. Camelli, S. Appanaboyina, J. D. Baum, E. L. Mestreau, and O. A. Soto, "Adaptive embedded and immersed unstructured grid techniques," *Comput. Methods Appl. Mech. Eng.*, vol. 197, nos. 25–28, pp. 2173–2197, Apr. 2008.

[20] Y. Chien, A. Ecer, H. Akay, S. Secer, and R. Blech, "Communication cost estimation for parallel CFD using variable time-stepping algorithms," *Comput. Methods Appl. Mech. Eng.*, vol. 190, nos. 11–12, pp. 1379–1389, Dec. 2000.

[21] B. E. Launder and D. B. Spalding, "The numerical computation of turbulent flows," *Comput. Methods Appl. Mech. Eng.*, vol. 3, pp. 269–289, Mar. 1974.

[22] V. Yakhot, S. A. Orszag, S. Thangam, T. B. Gatski, and C. G. Speziale, "Development of turbulence models for shear flows by a double expansion technique," *Phys. Fluids A, Fluid Dyn.*, vol. 4, no. 7, pp. 1510–1520, Jul. 1992.

[23] T.-H. Shih, W. W. Liou, A. Shabbir, Z. Yang, and J. Zhu, "A new k-ϵ eddy viscosity model for high reynolds number turbulent flows," *Comput. Fluids*, vol. 24, no. 3, pp. 227–238, Mar. 1995.

[24] T. Stathopoulos, "Computational wind engineering: Past achievements and future challenges," *J. Wind Eng. Ind. Aerody.*, vols. 67–68, pp. 509–532, Apr. 1997.

[25] P. Richards and R. Hoxey, "Appropriate boundary conditions for computational wind engineering models using the k-ϵ turbulence model," *J. Wind Eng. Ind. Aerody.*, vols. 46–47, pp. 145–153, 1993.

[26] S. B. Pope, *Turbulent Flows*. Cambridge, U.K.: Cambridge Univ. Press, 2000.

HAIMING ZHENG received the Ph.D. degree from the Shanghai University of Science and Technology, in 2006. He is currently an Associate Professor with the Department of Machinery of North China Electric Power University. He mainly studies optical mechanical and electrical monitoring, smoke monitoring, and more than 60 academic articles. He has been included in nearly 40 articles by SCI / EI / ISTP. Presided over and participated in nearly 40 vertical and horizontal projects, and obtained more than 20 patents.

SHUAI LI is currently pursuing the master's degree in mechanical structure design of optical mechanical and electrical instruments with the Mechanical Engineering Department, North China Electric Power University.

JIAWEI YIN is currently pursuing the master's degree with the Mechanical Engineering Department, North China Electric Power University. His main research interests are multicomponent gas detection technology of ultraviolet difference spectrometer and spectral absorption algorithm.

● ● ●